Optimization of the synthesis process of an iron oxide nanocatalyst supported on activated carbon for the inactivation of *Ascaris* eggs in water using the heterogeneous Fenton-like reaction

Ariadna A. Morales-Pérez, Pablo Maravilla, Myriam Solís-López, Rafael Schouwenaars, Alfonso Durán-Moreno and Rosa-María Ramírez-Zamora

ABSTRACT

An experimental design methodology was used to optimize the synthesis of an iron-supported nanocatalyst as well as the inactivation process of *Ascaris* eggs (Ae) using this material. A factor screening design was used for identifying the significant experimental factors for nanocatalyst support (supported %Fe, (w/w), temperature and time of calcination) and for the inactivation process called the heterogeneous Fenton-like reaction (H_2O_2 dose, mass ratio Fe/H_2O_2, pH and reaction time). The optimization of the significant factors was carried out using a face-centered central composite design. The optimal operating conditions for both processes were estimated with a statistical model and implemented experimentally with five replicates. The predicted value of the Ae inactivation rate was close to the laboratory results. At the optimal operating conditions of the nanocatalyst production and Ae inactivation process, the *Ascaris* ova showed genomic damage to the point that no cell reparation was possible showing that this advanced oxidation process was highly efficient for inactivating this pathogen.

Key words | *Ascaris* inactivation, experimental design, Fenton reaction, helminth egg, iron nanoparticles

Ariadna A. Morales-Pérez
Myriam Solís-López
Rosa-María Ramírez-Zamora (corresponding author)
Instituto de Ingeniería,
Universidad Nacional Autónoma de México,
México D.F., México
E-mail: *rramirezz@iingen.unam.mx*

Pablo Maravilla
Departamento de Ecología de Agentes Patógenos,
Hospital General Dr. Manuel Gea González, SSA,
México D.F. 14000, México

Rafael Schouwenaars
Departamento de Materiales y Manufactura, DIMEI,
Universidad Nacional Autónoma de México,
México D.F., México

Alfonso Durán-Moreno
Facultad de Química,
Universidad Nacional Autónoma de México, Cd. Universitaria, Coyoacán,
México, D. F. 04510, México

INTRODUCTION

The use of wastewater for irrigation is an established practice in many countries around the world because it is an important source of water and nutrients (Aladawi *et al.* 2006; Jimenez 2007). However, this leads to the proliferation of helminthoses and other water-borne diseases (Scott 2008). In developing countries the reuse of wastewater for the irrigation of crops represents a serious public health risk due to the high helminth egg (He) content (6–840 He/L, of which up to 90% are generally *Ascaris* eggs) (Jimenez 2007), which is significantly higher than the value recommended by the World Health Organization (≤0.1 He/L) for this purpose (Blumenthal *et al.* 2000).

Disinfection of treated wastewater is still carried out mainly using ozone or chlorine and its derivatives. But none of these disinfection reagents are effective for efficiently inactivating highly resistant pathogens such as helminth eggs (De Souza *et al.* 2011). In addition, these disinfection techniques are sensitive to environmental conditions such as temperature and pH and they are also known to generate carcinogenic by-products (Tahri *et al.* 2010).

Currently, the use of ionizing irradiation (e.g., ultraviolet, electron beam accelerators (β-rays) and gamma irradiation) is being evaluated as an alternative disinfection method (Aladawi *et al.* 2006; Hijnen *et al.* 2006; Tahri *et al.* 2010). However, its general application has been hampered because of the high costs, poor reliability of the equipment, maintenance problems and the advent of chlorination (Wolfe 1990). This has motivated the development of efficient and technically feasible removal processes. Among the processes currently in development, the Fenton reagent has emerged as a very attractive, environment-friendly technology for water disinfection.

doi: 10.2166/wst.2015.576

The classic Fenton reaction is an advanced oxidation process (AOP) that generates reactive oxygen species (ROS) ($^{\bullet}OH$, $O_2^{-\bullet}$, $O_2^{-\bullet}$ and $R-OO^{\bullet}$) using a mixture of two solutions: a reducing transition metal (Fe^{2+}, Cu^{+}, Co^{2+}, Mn^{3+}) and hydrogen peroxide (Fenton 1894). Fe(II) salts are commonly used because of their cost, availability and efficiency, particularly ferrous sulfate (Pignatello *et al.* 2006). When a non-Fe(II) transition metal is used, the reaction is known as the Fenton-like reaction. The hydroxyl radical ($^{\bullet}OH$), one of the most powerful oxidants (standard oxide reduction potential = 2.8 V), is the main ROS generated by the Fenton reaction.

A high inactivation rate (>99.999%) of *Ascaris suum* eggs (Ae) was reported using the homogeneous Fenton reaction (Fe^{2+} and H_2O_2) (Bandala *et al.* 2011). Nevertheless, this process produces an extremely acidic (pH = 3) effluent and the catalyst (Fe^{2+} and Fe^{3+}) is lost as highly acidic sludge (hazardous waste). To avoid these problems, nanoparticles of iron species can be fixed on solid porous supports such as activated carbon. These materials, due to their large surface area, could be as efficient or even more than dissolved iron salts or homogeneous catalysts (Garrido-Ramírez *et al.* 2010). Also, this catalyst can be recovered and recirculated due to the magnetic properties of iron oxides. A first trial for developing such materials was described in an earlier paper (Morales *et al.* 2014). However, additional research is needed to optimize simultaneously the nanoparticle synthesis process and the operating conditions of the heterogeneous Fenton-like reaction. Therefore, the purpose of this work was to optimize simultaneously the method for nanocatalyst synthesis and the Ae inactivation process and to evaluate the influence of supported iron and the process variables on the inactivation of Ae present in water, by using the heterogeneous Fenton process with H_2O_2 and a novel iron oxide nanocatalyst supported on activated carbon, FeOx/C.

METHODS

Materials

For the synthesis trials, the support of the nanocatalyst was a granular activated carbon of mineral origin (LQ 1000, Carbochem Co.) with particle sizes ranging from 297 to 590 μm. An alcoholic solution of iron 0.63 M was prepared using $Fe(NO_3)_3{\cdot}9H_2O$ (99%, Merck) and isopropyl alcohol (grade HPLC, Burdick and Jackson), as iron source and solvent, respectively.

For the inactivation tests, hydrogen peroxide at 30% (w/w) (J. T. Baker) was used. A stock suspension of Ae was prepared in a 0.5% formalin solution with eggs extracted from the uterus of female worms; this suspension, with 92% of initial viability, was stored at 4 °C prior to use. The initial viability of Ae was determined by two techniques, incubation and staining (De Victorica & Galván 2003).

Preparation of the iron oxide nanocatalyst supported on activated carbon

All nanocatalysts were produced using the technique reported by Morales *et al.* (2014). It consists of the incipient impregnation technique, using isopropyl alcohol as dissolvent and chelating agent of the iron salt, and an ultrasonic treatment. For the incipient impregnation process, 1.28 mL of an alcohol iron solution were added to 1 g of activated carbon (C) by dripping from a syringe and mixing continuously. The conditions for preparing a nanocatalyst with a supported %Fe in (w/w) are shown in Table 1. After this, 30 minutes of ultrasonic treatment (Bransonic 2510R-MT, 100 W and 42 kHz ± 6%) was applied for improving the dispersion of the chelated iron salt; this corresponds to the optimum time as reported by Nagao *et al.* (2007). Finally, to produce the FeOx nanoparticles, the sample was heated at a given calcination temperature (TC) during a given calcination time (tc) as established in the design presented in Table 1, and using N_2 as a carrier gas (30 cm^3/min) in a multifunction system (RIG-100/ISRI). The gas emissions from iron nitrate decomposition during preparation of the nanocatalyst was analyzed in-line by mass spectrometry (Hiden Analitical Ltd).

Inactivation trials of *Ascaris* eggs

The optimization process was developed in two stages. In the first stage, inactivation trials were carried out using a factor

Table 1 | Levels of factors selected in the experiment (factor screening)

	Level	
Experimental factor	**−1**	**1**
For the inactivation Ae process		
B = H_2O_2 dose, Dp (mg/L)	61.64	213.36
C = Fe/H_2O_2 mass ratio Rr	0.067	0.335
D = pH	3	7
For the synthesis catalyst process		
A = supported %Fe (w/w)	1	4.5
E = calcination temperature, TC (°C)	103	232
F = calcination time, tc (min)	26.76	213.24
G = reaction time, tr (min)	79.5	160.5

screening experimental design with two levels for each factor. The evaluated factors for the synthesis process were: supported % Fe (w/w), TC and tc, and for the Ae inactivation process were: H_2O_2 dose (Dp), mass ratio Fe/H_2O_2 (Rr), pH and reaction time (tr). Table 1 shows the coded and natural values of these factors.

The low and high values were set up using previously reported data for the heterogeneous Fenton reaction. The experiments were executed in randomized order. In this stage, 32 trials were performed in duplicate.

In the second stage, after identifying the significant factors, the synthesis and inactivation processes were optimized simultaneously using a face-centered central composite design. This design consists of the following parts: (1) a full factorial design; (2) an additional design, often a star design in which experimental points are at a distance α from its center; and (3) a central point (Almeida *et al.* 2008). All non-significant factors were constant in these 52 Ae inactivation experiments (26 factor combinations executed in duplicate).

In both experimental stages, all batch experiments were performed using 500 mL of laboratory-prepared suspension containing 2 Ae/mL. Although in Mexico the helminth egg content ranges from 6 to 840 He/L, in some other developing countries concentrations near 3,000 He/L (or 3 He/mL) have been found (Drechsel *et al.* 2009). Nonetheless, the leading concern is that, to properly determine the viability of the eggs by means of the staining technique, it is advisable to take a volume of 50 mL of sample with a concentration of 2 Ae/mL. The pH values of the suspensions were adjusted with 0.1 M H_2SO_4 and 0.1 M NaOH solutions. All experiments were carried out in stirred and covered reactors for the homogenization of samples and to avoid the photochemical decomposition of hydrogen peroxide. At the end of the reaction time, the oxidizing action of the hydrogen peroxide residual and ROS was quenched by adding 0.1 mL of a 0.1 N sodium thiosulphate solution. Subsequently, three samples of 50 mL were collected and filtered on nitrocellulose membranes (8.0 μm pore). The viability of Ae was determined using the vital staining procedure proposed by De Victorica & Galván (2003). The viability and inactivation percentages were calculated using the following equations:

$$\%\,\text{Ae viability} = \frac{\text{viable } Ascaris \text{ eggs}}{\text{total } Ascaris \text{ eggs}} \times 100 \quad (1)$$

$$\%\,\text{of Ae inactivation} = \frac{(\%\,\text{Ae viability})_{\text{initial}} - (\%\,\text{Ae viability})_{\text{final}}}{(\%\,\text{Ae viability})_{\text{initial}}} \times 100 \quad (2)$$

In addition, for the tests performed at the optimal operating conditions, RNA/DNA and whole proteins were extracted from Ae before and after the heterogeneous Fenton-like reaction, using a commercial kit (Puregene™kit, Gentra Systems, Germany) with inhibitors of endogenous nucleases and proteases to preserve the integrity of RNA/DNA and proteins in the samples. For RNA/DNA extraction, manufacturer's protocol was followed, a precipitation with isopropanol was performed and concentrations were determined spectrophotometrically. Samples were submitted to electrophoresis and nucleic acids were visualized by ethidium bromide staining on a 0.8% agarose gel. For protein analysis, a saline lysis buffer was used to disrupt Ae and to obtain a crude extract; proteins were quantified by Bradford method and analyzed by electrophoresis using 10% acrylamide gel under reducing conditions and stained by Coomassie blue stain.

Characterization of the optimum nanocatalyst

The optimum FeOx/C nanocatalyst was characterized in triplicate. The diameter of iron oxide particles present in this nanocatalyst was determined by transmission electron microscopy (TEM) images, recorded with a JEOL JEM-2010 microscope and the ImageJ® version 1.32 software. The total iron content was measured by atomic absorption spectroscopy by means of a Spectra AA (Varian) model 220 FS spectrophotometer after acid digestion. The specific surface area was determined using N_2 adsorption/desorption isotherms at 77 K with a BelSorp mini II analyzer, after outgasing of the samples at 80 °C for 12 h under nitrogen atmosphere.

The morphology and the dispersion degree of the iron oxides in the nanocatalyst were observed by scanning electron microscopy (SEM) with a JEOL JSM-5900LV microscope equipped with an energy dispersive spectrometer (EDS). Only the support material and the material that showed the best performance in the inactivation trial of Ae were characterized.

RESULTS AND DISCUSSION

Inactivation trials of *Ascaris* eggs for factor screening experimental design

In the first stage, only the individual effect of calcination time showed a significant influence (p-value < 0.05) at 95% confidence level on the Ae inactivation rate. Also, the majority of interactions of the evaluated factors showed a significant influence on this process (Figure 1).

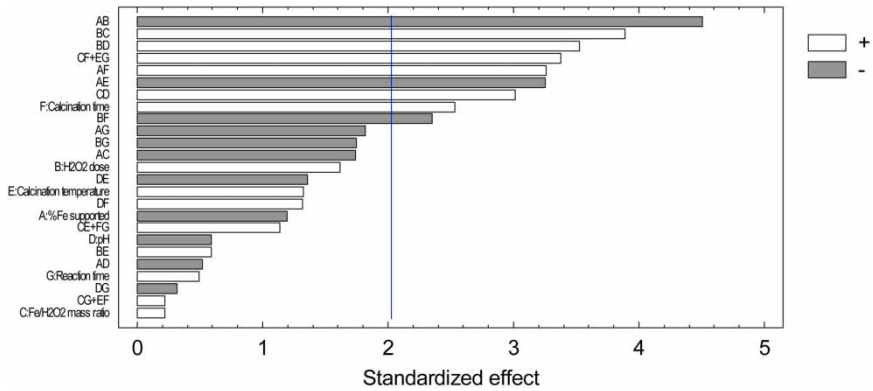

Figure 1 | Standardized Pareto chart of the factor screening design for the Ae inactivation process using the heterogeneous Fenton-like reaction with FeOx/C nanocatalysts.

Table 2 | Experimental matrix for optimization of the FeOx/C nanocatalyst method and the Ae inactivation process

	Factor									% Ae inactivation		
Test	A	B	C	D	Rr (m/m)	TC (°C)	tc (min)	Tr (min)	Supported %Fe (w/w) ($n = 3$)	Block 1	Block 2	Average
1	0	0	0	0	0.201	168	120	120.0	3.863 ± 0.10	40.8	51.6	46.21 ± 7.62
2	−1	0	0	0	0.067	168	120	120.0	3.863 ± 0.10	49.9	47.4	48.68 ± 1.77
3	1	−1	−1	1	0.335	103	26.76	160.5	3.454 ± 0.03	46.5	47.3	46.90 ± 0.54
4	0	0	0	−1	0.201	168	120	79.5	3.863 ± 0.10	44.9	49.2	47.02 ± 3.05
5	−1	1	−1	1	0.067	232	26.76	160.5	4.130 ± 0.23	46.3	40.7	43.50 ± 4.01
6	0	0	1	0	0.201	168	213.2	120.0	3.947 ± 0.28	39.6	51.2	45.4 ± 8.24
7	0	0	0	0	0.201	168	120	120.0	3.863 ± 0.10	37.1	47.6	42.31 ± 7.43
8	−1	−1	1	1	0.067	103	213.2	160.5	3.714 ± 0.11	81.4	76.2	**78.79 ± 3.72**
9	0	1	0	0	0.201	232	120	120.0	3.984 ± 0.40	57.1	54.3	55.69 ± 2.01
10	−1	−1	−1	−1	0.067	103	26.76	79.5	4.275 ± 0.27	43.1	43.5	43.29 ± 0.29
11	−1	1	1	−1	0.067	232	213.2	79.5	3.614 ± 0.09	50.0	43.7	46.85 ± 4.47
12	−1	1	1	1	0.067	232	213.2	160.5	4.189 ± 0.05	50.6	51.6	51.07 ± 0.74
13	1	1	1	1	0.335	232	213.2	160.5	4.189 ± 0.05	40.1	41.1	40.62 ± 0.70
14	−1	1	−1	−1	0.067	232	26.76	79.5	4.130 ± 0.23	31.3	27.8	29.59 ± 2.48
15	−1	−1	1	−1	0.067	103	213.2	79.5	3.970 ± 0.09	44.0	41.5	42.75 ± 1.82
16	1	0	0	0	0.335	168	120	120.0	3.863 ± 0.10	47.6	58.6	53.11 ± 7.77
17	1	1	−1	−1	0.335	232	26.76	79.5	3.953 ± 0.11	51.7	53.4	52.54 ± 1.22
18	0	−1	0	0	0.201	103	120	120.0	3.617 ± 0.07	75.6	73.5	74.54 ± 1.44
19	1	−1	1	1	0.335	103	213.2	160.5	3.970 ± 0.09	67.7	63.7	65.71 ± 2.85
20	1	1	−1	1	0.335	232	26.76	160.5	4.130 ± 0.23	60.5	61.5	60.98 ± 0.71
21	1	−1	−1	−1	0.335	103	26.76	79.5	4.275 ± 0.27	59.4	59.3	59.34 ± 0.11
22	0	0	−1	0	0.201	168	26.76	120.0	3.717 ± 0.16	66.4	67.1	66.75 ± 0.53
23	−1	−1	−1	1	0.067	103	26.76	160.5	4.275 ± 0.27	73.8	63.3	68.55 ± 7.38
24	0	0	0	1	0.201	168	120	160.5	3.863 ± 0.10	68.9	57.8	63.35 ± 7.82
25	1	1	1	−1	0.335	232	213.2	79.5	4.189 ± 0.05	71.7	72.0	71.82 ± 0.23
26	1	−1	1	−1	0.335	103	213.2	79.5	3.970 ± 0.09	70.7	84.4	77.55 ± 9.75

The results of these trials revealed that it is possible to work at a neutral pH value for obtaining a high Ae inactivation efficiency. This fact represents an important advantage with respect to the homogeneous Fenton reaction (Ramírez *et al.* 2006) and the ozonation method (Orta *et al.* 2004), since these processes were only effective for Ae inactivation at strongly acidic pH (3–4). Also, at low Dp (61.64 mg/L) it was possible to obtain a high Ae inactivation percentage (78.66 ± 3.05%), very close to the result obtained using a Dp value 3.5 times higher (Dp = 213.36 mg/L, % inactivation of Ae = 80.85 ± 0.0%); the higher value can have a negative impact on the process cost. Thus, for the optimization of this process (second stage), it was decided to use constant values of Dp (61.64 mg/L), reaction pH (7) and supported %Fe (4.5% w/w).

Table 3 | ANOVA of the Ae inactivation results

Source	Sum of squares	Df	Mean square	F-ratio	*p*-value
A: Rr	634.2	1	634.2	6.79	**0.0132**
B: TC	1219.17	1	1219.17	13.06	**0.0009**
C: tc	268.41	1	268.41	2.87	0.0986
D: tr	263.52	1	263.52	2.82	0.1016
AA	150.73	1	150.73	1.61	0.2120
AB	189.15	1	189.15	2.03	0.1633
AC	0.21	1	0.21	0.00	0.9623
AD	2003.44	1	2003.44	21.46	**0.0000**
BB	398.92	1	398.92	4.27	**0.0460**
BC	65.55	1	65.55	0.70	0.4076
BD	216.32	1	216.32	2.32	0.1367
CC	0.26	1	0.26	0.00	0.9583
CD	180.5	1	180.5	1.93	0.1730
DD	6.19	1	6.19	0.07	0.7982
Blocks	3.05	1	3.05	0.03	0.8575
Total error	3361.38	36	93.37		

Optimization of the nanocatalyst method and the *Ascaris* eggs inactivation process

The results obtained in the second experimental design are shown in Table 2. A large interval of inactivation percentages (27.8 at 84.4%) was obtained in the 52 trials (26 trials with a duplicate).

The Statgraphics version XV Centurion software was used for performing the statistical analysis of data obtained for screening or determining the significant factors with statistical influence on the Ae inactivation percentage. The complete analysis included: (1) analysis of variance (ANOVA) for percent inactivation of Ae; (2) standardized Pareto chart for the Ae inactivation rate; and (3) regression coefficients for the Ae inactivation rate. Table 3 shows the results of the ANOVA test to determine the statistical significance of each effect on the Ae inactivation process, by comparing the mean square against an estimate of the experimental error.

In this case, four effects (TC, Rr and two interactions: Rr with tr and TC–TC) showed *p*-values lower than 0.05, indicating that they had a statistical significance at a 95% confidence level. The *R*-squared statistic indicates that the model as fitted explains 62.10% of the variability in the Ae inactivation rate (%).

Figure 2 shows the Pareto chart graph, which indicates the type of influence of each significant effect on the Ae inactivation process.

In the evaluated interval, the Rr factor produced a positive effect on the process. As can be expected, an increase of Rr enhanced the Ae inactivation rate because if more iron is available for the reaction, more ROS can be produced. But, at large tr, the ROS can interact with themselves and a

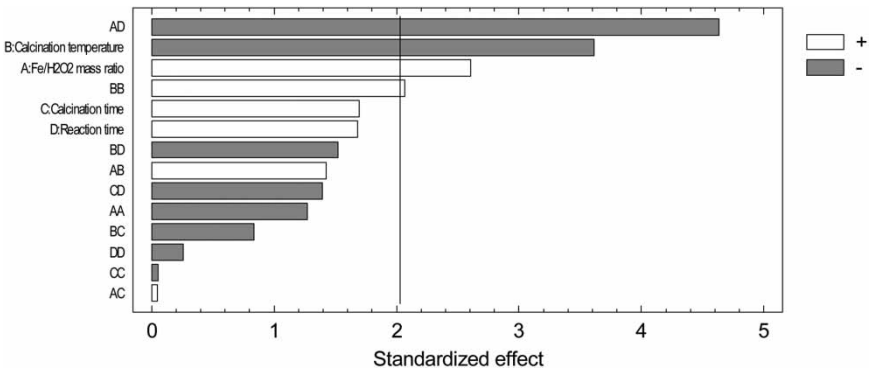

Figure 2 | Standardized Pareto chart of data obtained for optimizing the Ae inactivation rate (%).

recombination process is possible, which diminishes their inactivation action. For this reason the interaction Rr–tr can produce an adverse effect.

On the other hand, TC showed a negative effect on the Ae inactivation process. This could be because, at values of temperature higher than the Tamman temperature (Chen & Zhang 1992), the produced nanoparticles can move freely on the activated carbon surface, generating large clusters with lower specific surface area than nanoparticles of the catalyst. As a consequence, a loss of active sites for the ROS production reaction is observed.

The inactivation data were fitted to Equation (1) for estimating the optimal operating conditions:

$$\begin{aligned}&\text{Ae inactivation (\%)}\\&= 53.29 + 4.2Rr - 5.82TC + 2.73tc + 2.71tr - 5.42Rr^2\\&\quad + 2.43RrTC + 0.08Rrtc - 7.91Rrtr + 8.82TC^2 - 1.43TCtc\\&\quad - 2.6TCtr - 0.22tc^2 - 2.38tctr - 1.1tr^2 \qquad (3)\end{aligned}$$

where the values of factors are given in coded units [−1, 1].

The optimal values for maximizing the Ae inactivation rate were estimated using this statistical model. The calculated value of the maximum inactivation percentage was 75.32%. Table 4 shows the coded and natural values of factors for maximizing inactivation of Ae.

Synthesis of the nanocatalyst under optimal conditions

The optimum nanocatalyst was synthesized using the operating conditions given in Table 4. The Ae inactivation rate was determined five times at these optimal calculated conditions. In this case, the Ae inactivation rate was determined by using two techniques, incubation and staining (De Victorica & Galván 2003), and found to be 72.15 ± 5.37% (by staining) and 70.5 ± 2.91% (by incubation). Both results were very close to the estimated value.

Also, two additional trials were carried out for evaluating the contributions of the nanocatalyst and hydrogen peroxide on the Ae inactivation process separately, since the mineral carbon used as support contains iron and thus could also act as catalyst. For this reason, hydrogen peroxide alone and hydrogen peroxide combined with activated carbon were

Table 4 | Optimal coded and natural values of factors for the synthesis and Ae inactivation process using the heterogeneous Fenton-type reaction with FeOx/C supported nanocatalyst

Factor	Code value	Real value
Factor A: Rr	−0.57	0.126 mg/mg
Factor B: TC	−1.00	103 °C
Factor C: tc	1.0	213.2 min
Factor D: tr	1.0	160.5 min
Constant values		
Supported %Fe (w/w)		4.5%
Dp		61.64 mg/L
pH		7

Table 5 | Experimental values obtained at Ae inactivation optimal conditions

	Ae inactivation (%) ($n = 5$)	Consumed H_2O_2 (%) ($n = 5$)	Lixiviated Fe (ppm) ($n = 5$)
$FeOx/C + H_2O_2$	72.15 ± 5.37	45.8 ± 3.8	0.02 ± 0.01
$C + H_2O_2$	17.53 ± 3.40	64.3 ± 3.1	0.04 ± 0.02
H_2O_2	14.18 ± 7.97	31.8 ± 4.8	–

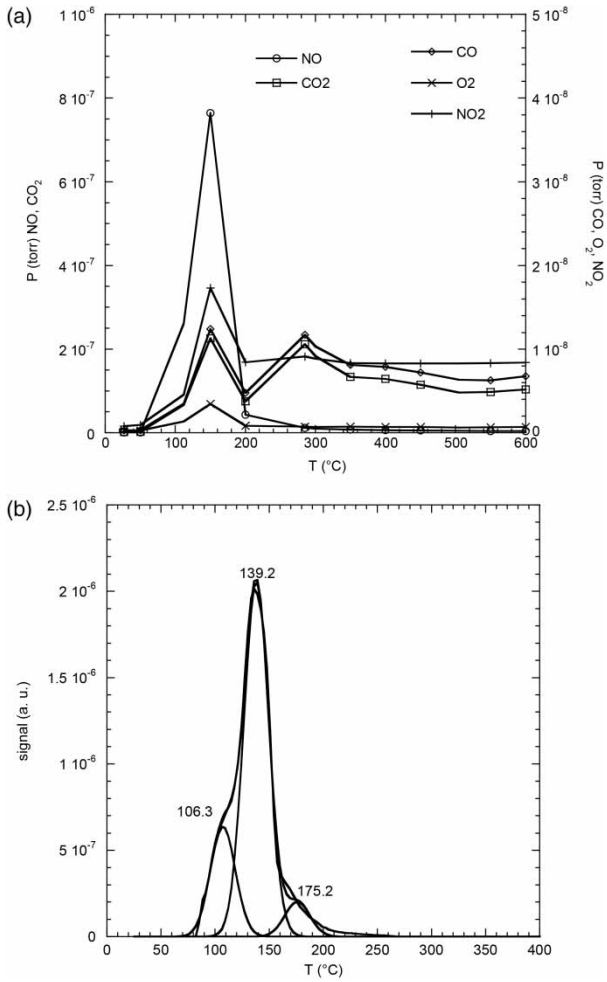

Figure 3 | (a) Mass profile emissions from iron nitrate decomposition, supported with isopropyl alcohol on activated carbon. (b) Deconvolution of NO mass profile.

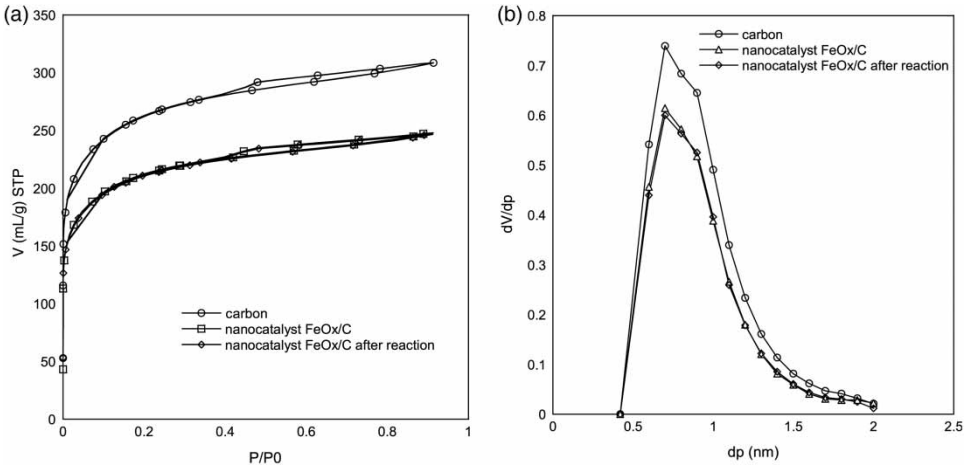

Figure 4 | (a) Nitrogen sorption and desorption isotherms of the optimum nanocatalyst at 77 K; (b) microporous distribution.

evaluated in Ae oxidation trials (Table 5). The Ae inactivation rate increased 4.12 times by incorporating iron oxide nanoparticles on the activated carbon particles, with respect to the result obtained using the activated carbon plus H_2O_2. Also, using H_2O_2 alone, only one-fifth of the total inactivation value was obtained as compared to what was achieved with the optimized heterogeneous Fenton process.

Characterization of the optimum nanocatalyst

The iron contents of the activated carbon (support) and the optimum synthesized nanocatalyst (FeOx/C) were 0.83 ± 0.11% w/w and 3.97 ± 0.09% w/w, respectively.

Figure 3(a) shows the mass profiles with NO and NO_2 emissions from iron nitrate decomposition and CO and CO_2 emissions from isopropyl alcohol decomposition, which was used as a solvent in the synthesis of nanocatalysts. The deconvolution of the NO profile (Figure 3(b)) shows three species formed with maximal temperatures of 107, 138 and 176 °C. However, these species are not separated; a mixture of them is observed. Thus, it is possible that the activity is a function of a specific combination of the produced iron oxide species.

Figure 4(a) shows the nitrogen sorption and desorption isotherms of carbon (support) and nanocatalyst FeOx/C. According to the IUPAC classification (Sing 1982), the isotherm was type I, which is characteristic of microporous solids (Leofanti *et al.* 1998). A microporous distribution (pore diameter < 2 nm) is shown in Figure 4(b). Notably, the relative abundance of pores with 0.7 nm diameter decreased after the synthesis process, probably due to the deposition of nanoparticles which obstruct these pores.

Table 6 shows the Brunauer–Emmett–Teller (BET) area and porous volume (Vp) measured for the support nanocatalyst (activated carbon) and the optimum FeOx/C nanocatalyst. After pre-treatment, the nanocatalyst support lost 19.05% of specific surface area (BET area) and 8.7% of total Vp; this probably due to the applied thermal pretreatment. On the other hand, 10.8% of the support area was covered with supported FeOx nanoparticles. The reduction of Vp indicates that nanoparticles were also deposited inside the carbon pores.

The nanocatalyst support showed particles with sizes ranging from 297 to 590 μm. These particles had a lengthened shape and wrinkled surface with visible porosity (Figure 5(a)). Several crystal and amorphous structures can be observed distributed at the particle surface (Figure 5(b)) because the activated carbon was of mineral origin. Si, Ti, Au, Zr, Cu, Na, P and Fe were identified by EDS.

Figures 5(c) and (d) show some TEM micrographs recorded using a QBSD detector. The iron nanoparticles

Table 6 | Textural properties of support and nanocatalyst

	BET area (m^2/g) ($n = 2$)	Vp (cm^3/g) ($n = 2$)
Activated carbon (nanocatalyst support) before thermal pretreatment	936.475 ± 2.52	0.508 ± 0.0
Activated carbon after thermal pretreatment	758.40 ± 32.07	0.464 ± 0.019
Nanocatalyst FeOx/C before Ae inactivation reaction	676.37 ± 31.11	0.377 ± 0.009
Nanocatalyst FeOx/C after Ae inactivation reaction	609.10 ± 83.74	0.348 ± 0.047

Figure 5 | SEM micrographs of activated carbon or nanocatalyst support (a) and (b); TEM micrographs of the optimum nanocatalyst FeOx/C (c) and (d).

were observed in association with the activated carbon pores (Figure 5(c)); this fact is in agreement with the nitrogen adsorption results, but also other nanoparticles were observed on the activated carbon surface (Figure 5(d)). The nanoparticles observed in Figure 5(c) and 5(d) show sizes of 2.5 nm, 3.5 nm, 4.2 nm, 4.4 nm, 7.5 nm and 14.9 nm, respectively.

Cellular mechanisms of inactivation

Genomic DNA and RNA band profiles (28S, 18S and tRNA) were observed in samples before treatment, but RNA bands disappeared in samples that were treated by the heterogeneous Fenton-like reaction. Likewise, samples before this process showed some proteins of high molecular weight (>200 kDa); in contrast, these bands were not observed in treated samples. Therefore, these results suggest that ROS generated by the heterogeneous Fenton like reaction degraded the RNA and high molecular weight proteins of Ae; this was probably due to a polypeptide oxidation mechanism suggested by Imlay (2008). In contrast, DNA did not show any degradation by this process, but alterations in the cellular metabolism of Ae were evident; the regeneration of genetic material through reparation mechanisms is not possible without RNA and proteins, since both are essential elements necessary for the genomic reparation (Jomova & Valko 2011); therefore, the observed damage is irreversible and consequently induces cellular death, which is the cause of the inactivation of the Ae.

Comparison with other Ae inactivation methods

Table 7 shows a comparison of the system proposed in this work with respect to other similar reported systems.

The three main advantages of the proposed system are: (1) it can work at neutral pH, avoiding the problem of acidic by-products which have to be treated afterwards; (2) it does not require a light source; and (3) iron loss is not significant. Considering that hydrogen peroxide is consumed in the process, it is interesting to determine the process efficiency in terms of the Ae inactivation rate (%) per mg of supplied H_2O_2. In this sense, the proposed system showed an efficiency (7.8% inactivation/mg H_2O_2) significantly higher than the current values reported for all the similar Ae inactivation methods. The low H_2O_2 consumption is beneficial to the process cost.

CONCLUSIONS

The simultaneous optimization of the FeOx/C nanocatalyst synthesis method and the Ae inactivation process was

Table 7 | Comparison with other reported Ae inactivation methods

	Homogeneous Fenton					Heterogeneous Fenton	
	Dark		UV light	Solar		Dark	
Reference	Ramírez *et al.* (2006)	Escobar-Megchún *et al.* (2014)	García *et al.* (2008)	Guísar *et al.* (2007)	Bandala *et al.* (2011)	Morales *et al.* (2014)	This work
Type of catalyst	Fe^{3+}	Fe^{2+}	Fe^{2+}	Fe	Fe^{2+}	FeOx/C	FeOx/C
% inactivation/mg H_2O_2	3.34	1.216	NR	0.41	0.18	4.3	7.80
Reaction pH	3	6	3	3	3	4	7
H_2O_2 (mg/L) dose	40	500	NR	2380	9520	28.64	61.6
Reaction time (min)	50	120	120	90	120	58	160.5
Mass ratio Fe/H_2O_2 (mg/mg)	10	0.549	NR	0.12	0.058	0.1	0.126

NR, no reported.

successfully performed in this work by means of experimental designs. From the results, the predicted optimal process and treatment conditions were used to produce an iron nanocatalyst supported on activated carbon, which showed an efficiency very close to the predicted one. The heterogeneous Fenton process developed here shows an efficiency which is similar to other AOPs, but produces no acidic by-products, does not suffer the loss of catalysts in sludges and has a lower H_2O_2 consumption than what has been reported in literature. At the cellular level, it was seen that the process causes damage to proteins of high molecular weight and destroys tRNA, which makes cell repair impossible.

ACKNOWLEDGEMENTS

The authors are grateful to CONACYT for the financial support under grant SEP-2004-C01-48097. They wish to thank Gustavo Fuentes Zurita from the Universidad Autónoma Metropolitana-Iztapalapa for the use of the RIG-100/ISRI equipment, Ivan Puente Lee from the Universidad Nacional Autónoma de México for the TEM and SEM analysis, Dr. Fernando Martínez and Dr Mirza Romero from Departamento de Ecología de Agentes Patógenos, Hospital General 'Dr. Manuel Gea González', SSA for the use of the Bioteck equipment and experimental help, respectively. Ariadna A. Morales thanks the CEP-UNAM for her PhD scholarship. R. Schouwenaars thanks DGAPA for support for his sabbatical leave under the PASPA program.

REFERENCES

Aladawi, M. A., Albarodi, H., Hammoudeh, A., Shamma, M. & Sharabi, N. 2006 Accelerated larvae development of *Ascaris lumbricoides* eggs with ultraviolet radiation. *Radiation Physics and Chemistry* **75** (1), 115–119.

Almeida, M., Erthal, R., Padua, E., Silveira, L. & Amélia, L. 2008 Review. Response surface methodology (RSM) as a tool for optimization in analytical chemistry. *Talanta* **76**, 965–977.

Bandala, E., González, L., de la Hoz, F., Pelaez, M., Dionysiou, D., Dunlop, P., Byrne, J. & Sanchez, J. 2011 Application of azo dyes as dosimetric indicators for enhanced photocatalytic solar disinfection (ENPHOSODIS). *Journal of Photochemistry and Photobiology A: Chemistry* **218**, 185–191.

Blumenthal, U., Duncan, D., Peassey, A., Ruíz-Palacios, G. & Stott, R. 2000 Guidelines for the microbiological quality of treated wastewater used in agriculture: recommendations for revising WHO guidelines. *Bulletin of the World Health Organization* **78** (9), 1104–1116. http://www.who.int/bulletin/archives/78(9)1104.pdf (accessed 23 October 2010).

Chen, Y. & Zhang, L. 1992 Surface interaction model of γ-alumina-supported metal oxides. *Catalysis Letters* **12**, 51–62.

De Souza, G. S. M. B., Rodrigues, L. A., De Oliveira, W. J., Chernicharo, C. A. L., Guimarães, M. P., Massara, C. L. & Gorssi, P. A. 2011 Disinfection of domestic effluents by gamma radiation: effects on the inactivation of *Ascaris lumbricoides* eggs. *Water Research* **45** (17), 5523–5528.

De Victorica, J. & Galván, M. 2003 Preliminary testing of a rapid coupled methodology for quantitation/viability determination of helminth eggs in raw and treated wastewater. *Water Research* **37** (6), 1278–1287.

Drechsel, P., Scott, C. A., Raschid-Sally, L., Redwood, M. & Bahri, A. 2009 Wastewater irrigation and health: Assessing and mitigating risk in low–income countries. http://hdl.handle.net/10625/41052.

Escobar-Megchún, S., Nájera-Aguilar, H., González-Hilerio, M., Gutiérrez-Jiménez, J., Gutiérrez-Hernández, F. &

Rojas-Valencia, M. 2014 Application of the Fenton process in the elimination of helminth eggs. *Journal of Water and Health* **12** (4), 722–726.

Fenton, H. J. H. 1894 Oxidation of tartaric acid in presence of iron. *Journal of the Chemical Society* **65**, 899–910.

García, J., Mejía, L., Bandala, E. & Corona, B. 2008 Inactivación de huevos de helminto mediante fotocatálisis homogénea (Inactivation of helminth eggs by homogeneous photocatalysis). *Aquaforum* **49**, 14–18.

Garrido-Ramírez, E., Theng, B. & Mora, M. 2010 Clays and oxide minerals as catalysts and nanocatalysts in Fenton-like reactions – a review. *Applied Clay Science* **47**, 182–192.

Guísar, R., Herrera, M., Bandala, E., García, J. & Vasquez, B. 2007 Inactivation of waterborne pathogens using solar photocatalysis. *Journal of Advanced Oxidation Technologies* **10**, 435–438.

Hijnen, W. A. M., Beerendonk, E. F. & Medema, G. J. 2006 Inactivation credit of UV radiation for viruses, bacteria and protozoan (oo)cysts in water: a review. *Water Research* **40** (1), 3–22.

Imlay, J. 2008 Cellular defenses against superoxide and hydrogen peroxide *Annual Review of Biochemistry* **77**, 755–776.

Jimenez, B. 2007 Helminth ova removal from wastewater for agriculture and aquaculture reuse. *Water Science & Technology* **55** (1), 485–493.

Jomova, K. & Valko, M. 2011 Advances in metal-induced oxidative stress and human disease. *Toxicology* **283**, 65–87.

Leofanti, G., Padovan, M., Tozzola, G. & Venturelli, B. 1998 Surface area and pore texture of catalysts. *Catalysis Today* **41**, 207–219.

Morales, A. A., Schouwenaars, R., Pfeiffer, H. & Ramirez-Zamora, R. M. 2014 Inactivation of *Ascaris* eggs in water using hydrogen peroxide and a Fenton type nanocatalyst (FeOx/C) synthesized by a novel hybrid production process. *Journal of Water and Health* **11** (3), 419–429.

Nagao, D., Shimazaki, Y., Saeki, S., Kobayashi, Y. & Konno, M. 2007 Effect of ultrasonic irradiation on carbon-supported Pt-Ru nanoparticles prepared at high metal concentration. *Colloid and Surfaces A* **302**, 623–627.

Orta De Velazquez, M., Martínez, J., Monje-Ramírez, I. & Rojas-Valencia, M. 2004 Destruction of helminth (*Ascaris suum*) eggs by ozone. *Ozone: Science and Engineering* **26**, 359–366.

Pignatello, J., Oliveros, E. & Mackay, A. 2006 Advanced oxidation processes for organic contaminant destruction based on the Fenton reaction and related chemistry. *Critical Reviews in Environmental Science and Technology* **36** (1), 1–84.

Ramírez, R., Galván, M., Gallardo, I., Rigas, F. & Durán, A. 2006 Viability reduction of parasites (*Ascaris* spp.) in water with photo-Fenton reaction via response surface methodology. *Water Practice & Technology* **1** (2), 1–8.

Scott, M. E. 2008 *Ascaris lumbricoides*: a review of its epidemiology and relationship to other infections. *Annales Nestlé* **66** (1), 7–22.

Sing, K. 1982 Reporting physisorption data for gas/solid systems with special reference to the determination of surface area and porosity. *Pure & Applied Chemical* **54** (11), 2201–2218.

Tahri, L., Elgarrouj, D., Zantar, S., Mouhib, M., Azmani, A. & Sayah, F. 2010 Wastewater treatment using gamma irradiation: Tétouan pilot station, Morocco. *Radiation Physics and Chemistry* **79** (4), 424–428.

Wolfe, R. L. 1990 Ultraviolet disinfection of potable water. *Environmental Science and Technology* **24** (6), 768–773.

First received 22 June 2015; accepted in revised form 28 October 2015. Available online 7 November 2015